Measurement of the Photodissociation Coefficient of NO_2 in the Atmosphere: I. Method and Surface Measurements

S. MADRONICH*, D. R. HASTIE, B. A. RIDLEY** and H. I. SCHIFF
Department of Chemistry, York University, Downsview, Ontario, Canada M3J 1P3

Abstract. An instrument, specifically designed for measurements from a balloon platform in the stratosphere, has been used to obtain ground-level values of the atmospheric photodissociation coefficient of nitrogen dioxide, J_{NO_2}. A typical clear-sky value is 8.0×10^{-3} s^{-1} when the solar zenith angle is 40°. Measurements were made as a function of solar zenith angle and correlated with a calibrated Eppley UV radiometer. It is shown that J_{NO_2} may be expressed as a simple function of the radiometer output so that estimates of J_{NO_2} can be made using just an upward looking radiometer to an accuracy of about 20%. The measurements are also found to be in good agreement with calculations of J_{NO_2} using a simplified isotropic multiple scattering computer routine.

Key words. J_{NO_2}, NO_2 photolysis, atmospheric photochemistry, J_{NO_2} measurement.

1. Introduction

Photolysis of NO_2 occurs at wavelengths less than 420 nm. Since solar radiation in this wavelength region is only partially absorbed by the atmosphere, this process plays an important, and somewhat ambivalent, role in atmospheric chemistry at all altitudes.

In the troposphere it is the main source of 'odd oxygen':

$$NO_2 + h\nu \longrightarrow NO + O. \qquad \text{(R1)}$$

The oxygen atoms lead to the production of ozone and other photo-oxidants.

In the stratosphere, by contrast, NO_2 provides a major loss or sink of 'odd oxygen', by the reaction:

$$NO_2 + O \longrightarrow NO + O_2. \qquad \text{(R2)}$$

The photolysis reaction (R1) is important in determining the partitioning of NO_x ($NO + NO_2$) in the daytime stratosphere. The steady state expression for this partitioning can be

* Present address: Aerochem Research Laboratories, PO Box 12 Princeton, NJ 08540, U.S.A.
** Present address: National Center for Atmospheric Research, PO Box 3000, Boulder, CO 80307, U.S.A.

represented by:

$$\frac{[NO_2]}{[NO]} = \frac{k_{NO,O_3}[O_3] + k_{NO,C\ell O}[C\ell O] + k_{NO,HO_2}[HO_2] + \ldots}{J_{NO_2} + k_{NO_2,O}[O] + \ldots} \quad (1)$$

where the k's are the rate coefficients for the bimolecular reactions indicated by the subscripts and J_{NO_2} is the photodissociation coefficient for reaction (R1). The first terms in each of the numerator and denominator dominate the right hand side of the equation.

The steady state is established, under typical insolation, with a time constant of several minutes, which is much shorter than characteristic transport time constants. Simultaneous measurements of NO, NO_2, O_3, and J_{NO_2} therefore afford a unique test for stratospheric chemistry. Such a set of measurements is the principal motivation for the development of the method for making *in situ* J_{NO_2} measurements described in this paper.

In the troposphere there is mounting evidence that additional oxidation terms may be required in the numerator of Equation (1).

In principle, J_{NO_2} can be calculated from the expression:

$$J_{NO_2} = \int_\lambda \sigma(\lambda)\,\phi(\lambda)\,F(\lambda)\,d\lambda \quad (2)$$

where $\sigma(\lambda)$ is the NO_2 absorption cross-section, $\phi(\lambda)$ the quantum efficiency of reaction (R1) and $F(\lambda)$ the solar actinic flux at the altitude of interest. Recent evaluations of $\sigma(\lambda)$ and $\phi(\lambda)$ are probably each accurate to 10% (JPL, 1982), and show some systematic differences from earlier measurements, with significant temperature dependences. The extraterrestrial solar flux in the relevant spectral region has also been reviewed (WMO, 1981), with measurements differing by as much as 20%. Moreover, a calculation of the actinic flux at the altitude under consideration must include the attenuation due to absorption by atmospheric gases and particles as well as the contributions from diffuse (scattered) radiation and reflections from clouds and the surface. The importance of these effects have been amply demonstrated (e.g., Luther and Gelinas, 1976; Mugnai *et al.*, 1979), but the computational complexity involved in treating them, especially at large zenith angles, and the uncertainties in parameterization of surface and cloud albedo and aerosol loading make a direct measurement of J_{NO_2} preferable for a test of Equation (1).

Previous methods used to measure J_{NO_2} in the troposphere (Jackson *et al.*, 1975; Zafonte *et al.*, 1972; Harvey *et al.*, 1977; Bahe *et al.*, 1980; Dickerson *et al.*, 1982) require knowledge of the kinetics of a number of reactions or the absolute concentrations of several species. The novel method to be described in this paper requires only measurements of the pressure in the photolysis cell. The only reaction which needs to be considered is the dimerization of NO_2 at low temperatures and is readily taken into account. Other reactions will be shown to make only small contributions to the uncertainty.

No measurements of the NO_2 photolysis rate in the stratosphere have yet been reported. The present paper describes an instrument designed to measure J_{NO_2}, *in situ*,

from a balloon platform. It also describes the results of surface measurements of J_{NO_2} made as part of the tests of the balloon instrument, and compares these measurements with some theoretical calculations, and with other tropospheric measurements. A subsequent paper will describe the results of the stratospheric measurements.

2. Experimental

The experimental method is based on the pressure increase which accompanies the photodissociation of NO_2 in a closed quartz cell. The primary photodissociation reaction (R1) is followed rapidly by (R2) and results in the net reaction:

$$2NO_2 + h\nu \longrightarrow 2NO + O_2$$

and the pressure increases.

Under typical daylight insolation, the photodissociation lifetime of NO_2 is greater than 60 s, which is orders of magnitude larger than the O atom chemical loss lifetime from reaction (R2) under typical cell pressures of a few torr. The oxygen atom concentration therefore reaches steady state rapidly and, to a close approximation, the disappearance of NO_2 is:

$$\frac{-\mathrm{d}[NO_2]}{\mathrm{d}t} = 2J_M[NO_2] \tag{3}$$

where J_M is the photodissociation coefficient in the cell and is to be distinguished from the atmospheric photodissociation coefficient, J_{NO_2}. The increase in cell pressure at time t, $\Delta P(t) = P(t) - P(0)$, is therefore related to J_M by:

$$-2J_M t = \ln\left[1 - \frac{2\Delta P(t)}{P(0)}\right] \tag{4}$$

where $P(0)$ is the initial NO_2 pressure.

The photodissociation coefficient of NO_2 at any position in the atmosphere, J_{NO_2}, may differ from J_M measured in the cell at an adjacent position, because of perturbations of the light by the apparatus. Moreover, other reactions may be occurring in the cell which may not be identical to those in the surrounding atmosphere. Consideration will be given to both these questions later in this paper.

3. Apparatus

The photolysis cell used in these studies was not optimized for groundbased measurements but could be readily modified to do so. It was designed specifically for use on stratospheric balloon payloads and a schematic is shown in Figure 1. The inner quartz photolysis cylinder, 1.0 cm ID, 1.6 cm OD and 57.8 cm in length, is enclosed by an outer quartz cylinder 3.3 cm ID, 3.9 cm OD and 60.9 cm in length and the annulus evacuated to better than 10^{-4} torr. The photolysis cell is connected by 0.22 cm ID tubing to inlet and outlet, latching, solenoid valves and to an absolute pressure transducer (Validyne,

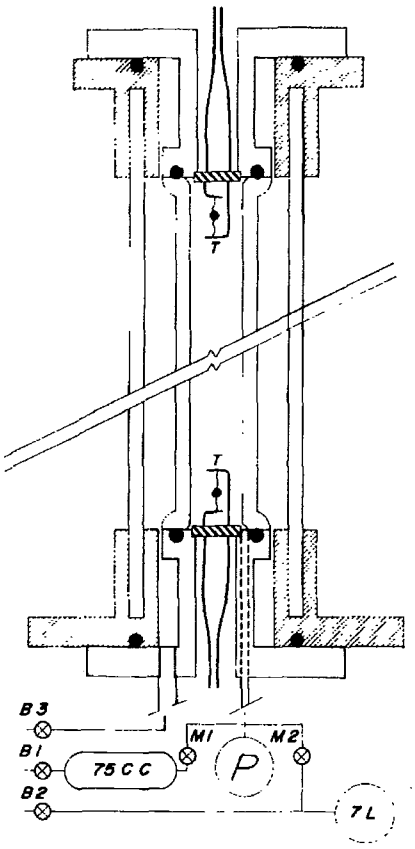

Fig. 1. Schematic of the photolysis cell. P – absolute pressure transducer; T – thermistors; $B1$, $B2$, $B3$ – bellows valves; $M1$, $M2$ – latching solenoid valves. Not shown is the insulating foam which shadows a small portion of the cell.

P24, 0–5 torr range). The 75 cc reservoir, containing NO_2 at about 70 torr, and the 7 l pre-evacuated tank, used for pumping the photolysis products from the cell after an experiment, are connected, through bellows valves, to ports outside the instrument for preliminary preparations. The reservoirs, valves and tubing are constructed of stainless steel; the vacuum connnections utilize nickel or viton gaskets. Teflon, silicon rubber and epoxy were avoided, since early tests showed that these materials exhibited adsorption effects when exposed to NO_2.

A mechanically-operated shutter is used to keep the photolysis cell in the dark prior to charging it with NO_2. The shutter is a lightweight, black-anodized, aluminum cylinder, 23 cm in diameter, equipped with light baffles at each end. The cell is shielded from light by raising the shutter on motor-driven lead screws. The shutter is disengaged from the lead screws and lowered gravitationally in about 1 s to expose the cell to ambient light. The shutter is covered externally with foam and lined internally with heaters, since, in cold stratospheric environments, the cell must be kept warm to minimize the dimerization of NO_2. The foam extends 4.3 cm above the bottom flange and 0.8 cm below the upper flange. For ground-based measurements described in this paper, no heating was used and the cell remained at ambient temperature.

The instrument electronics are designed to allow remote control of the solenoid valves, the shutter mechanism, and the heater. The cell pressure, temperatures at several locations in the instrument, the shutter position, and the status of the valves can be telemetered to the ground station.

NO_2 was prepared by reacting NO (Matheson CP grade, 99%) repeatedly with excess O_2 (Linde UHP Grade, 99.9%) and was purified by trap-to-trap distillation. The final condensate was composed entirely of white crystals at 77 K. Upon warming, the central half of the distillate was collected and stored in stainless steel containers at ambient temperature and at about 70 torr pressure.

4. Kinetic Considerations

In this section we will show that the occurrence of reactions other than those used to derive Equation (4) play a negligible role at NO_2 partial pressures of 1 torr or less and at temperatures near 298 K. The validity of Equation (4) was therefore tested experimentally in the laboratory by photolysing NO_2 at 1 torr and 298 K with light from a 500 Watt Xe arc lamp. In addition to measuring the total pressure as a function of time, the NO_2 concentration was simultaneously monitored by optical absorption at 430 nm. The photodissociation coefficient, J_M, determined from the pressure measurements was well within the 4% instrumental uncertainty of the value determined by the absorption method, confirming that J_M can be measured directly from the pressure increase under these experimental conditions.

However, some of our field experiments were conducted at lower cell temperatures and higher NO_2 pressures. Under these conditions small, but significant, amounts of dinitrogen tetroxide (N_2O_4) are produced by dimerization of NO_2 and Equation (4) must be modified accordingly.

The NO_2/N_2O_4 equilibrium is maintained by the rapid forward and reverse reactions

$$N_2O_4 \underset{}{\overset{M}{\rightleftharpoons}} 2NO_2 \qquad \text{(R3)}$$

where the equilibrium constant, K, is a strong function of temperature. The rates of change of NO_2 and N_2O_4 are related by:

$$\frac{d[N_2O_4]}{dt} = \frac{2[NO_2]}{K}\frac{d[NO_2]}{dt}. \qquad (5)$$

The disappearance of NO_2 during photolysis is then given by the rate equation:

$$-\frac{d[NO_2]}{dt} = \frac{2J_M[NO_2]}{1+(4/K)[NO_2]}. \qquad (6)$$

This equation is readily integrated and expressed in terms of $p_{NO_2}(t)$, the NO_2 partial pressure at time t:

$$-2J_M t = \ln\frac{p_{NO_2}(t)}{p_{NO_2}(0)} + \frac{4}{K}[p_{NO_2}(t) - p_{NO_2}(0)]. \qquad (7)$$

Equation (7) is the basic equation used to determine J_M. All of the quantities on the right-hand side can be determined from the total pressure, P, measured as a function of time if the gas mixture is assumed to consist entirely of NO_2, N_2O_4, NO and O_2.

From stoichiometry alone it can be shown that:

$$p_{N_2O_4}(0) = \frac{2}{3}\Delta P(\infty) - \frac{1}{3}P(0) \tag{8}$$

$$p_{NO_2}(0) = P(0) - p_{N_2O_4}(0) \tag{9}$$

$$K = p^2_{NO_2}(0)/p_{N_2O_4}(0) \tag{10}$$

$$p_{NO_2}(t) = \frac{1}{2}\left[4p^2_{NO_2}(0) + Kp_{NO_2}(0) + K^2/16 - 2K\Delta P(t)\right]^{1/2} - \frac{K}{8} \tag{11}$$

where $\Delta P(t)$ is the change in total pressure at time t and $\Delta P(\infty)$ is the pressure change after photolysis is essentially complete.

To test the validity of these expressions, photolysis experiments were conducted outdoors on different days for which the temperatures spanned the range from 0 to 26°C. Values of $p_{N_2O_4}(0)$ were calculated from the measured initial and final total pressure using Equation (8), which does not require a knowledge of the temperature; it need only be constant over the photolysis period. The calculated values were compared with the predicted values, obtained from the expression:

$$p_{N_2O_4}(0) = P(0) - \frac{K}{2}\left[\left(1 + \frac{4P(0)}{K}\right)^{1/2} - 1\right] \tag{12}$$

as derived from Equations (9) and (10) using published thermodynamic equilibrium constants for the temperature of each experiment. The results of this comparison are shown in Table I. Good agreement is noted over the entire temperature range.

Table I. N_2O_4 temperature study

$T \pm 2$ (°C)	$P(0)$ (torr)	$P_{N_2O_4}$	
		Experimental[a] (torr)	Theoretical[b] (torr)
0	1.8	0.24 ± 0.02	0.20 ± 0.03
2.5	3.00	0.41 ± 0.02	0.40 ± 0.04
2.5	1.62	0.14 ± 0.02	0.13 ± 0.02
3	2.34	0.21 ± 0.02	0.24 ± 0.03
11	1.51	0.05 ± 0.02	0.06 ± 0.01
11	1.57	0.08 ± 0.02	0.06 ± 0.01
12	1.62	0.06 ± 0.02	0.06 ± 0.01
14	1.62	0.06 ± 0.02	0.06 ± 0.01
26	1.91	0.03 ± 0.02	0.03 ± 0.01

[a] From Equation (8). [b] From Equation (12).

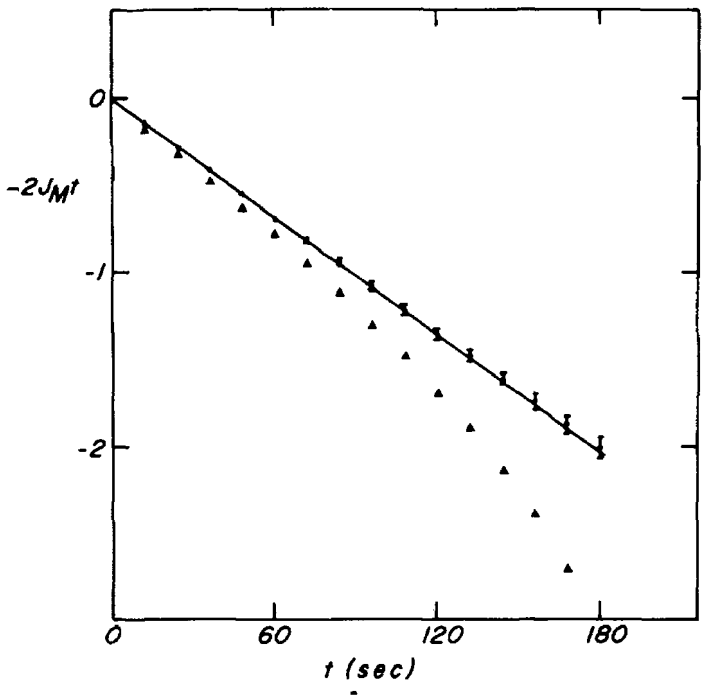

Fig. 2. (•) the right-hand side of Equation (7) and (▲), the right-hand side of Equation (4) plotted as a function of time for the data obtained on 27 March, 1981 at 14 : 58 EST.

Further support for the validity of the N_2O_4 correction is provided in Figure 2, which compares a plot of a typical data set using Equation (7), which corrects the pressure increase data for the presence of N_2O_4, with a plot of the same data using Equation (4), which neglects N_2O_4. The predicted linearity can be obtained over at least three 'e-folding' times when the N_2O_4 correction is applied.

Precise determinations of J_M therefore require attention to the presence of small amounts of N_2O_4. Other chemical reactions which may occur in the cell will now be considered.

Photodissociation of N_2O_4 is a possible perturbation to the basic kinetic scheme. Johnston and Graham (1974) have suggested two possible product channels:

$$N_2O_4 + h\nu \xrightarrow{J_4} 2NO_2 \tag{R4}$$

$$\xrightarrow{J_5} N_2O_3 + O \longrightarrow NO + NO_2 + O \tag{R5}$$

where (R4) simply leads to the re-establishment of the equilibrium while (R5) is followed by reaction of NO_2 with oxygen atoms. The reaction associated with NO production is energetically possible only for wavelengths shorter than 373 nm.

These reactions are readily incorporated into rate equation (6) which, upon integration, yields:

$$-2J_M t = \ln\left[\frac{p_{NO_2}(t)}{p_{NO_2}(0)}\right] + (1 - J_5/4J_M)\left[p_{NO_2}(t) - p_{NO_2}(0)\right]\frac{4}{K} \tag{13}$$

since $J_5 p_{N_2O_4}(t) \ll J_M p_{NO_2}(t)$. Except for the term $J_5/4J_M$, Equation (13) is identical to Equation (7). The value of J_5 was estimated from the N_2O_4 absorption cross-section (Johnston and Graham, 1974), the quantum yield for NO formation (Holmes and Daniels, 1934) and the extraterrestrial flux. This calculation gives $J_5 \simeq 5 \times 10^{-4}\ s^{-1}$, or about 7% of the J_M value for NO_2. The term $J_5/4J_M$ therefore represents a 1.5% decrease in the N_2O_4 correction which corresponds to an overestimation of 0.5% in J_M for the experiment in which $p_{N_2O_4}(0)$ was the largest.

Table II. Reactions of minor species

$2O$	+ M		$\rightarrow O_2$	+ M			
O	+ O_2	+ M		$\rightarrow O_3$	+ M		
O	+ NO	+ M		$\rightarrow NO_2$	+ M		
O	+ NO_2	+ M		$\rightarrow NO_3$	+ M		
NO_3	+ NO_2		$\rightarrow NO_2$	+ O_2		+ NO	
NO_3	+ NO		$\rightarrow 2NO_2$				
NO_3	+ NO_2	+ M		$\rightarrow N_2O_5$	+ M		
NO_3	+ $h\nu$		$\rightarrow NO_2$	+ O			
O_3	+ $h\nu$		$\rightarrow O_2$	+ O			
O_3	+ NO		$\rightarrow NO_2$	+ O_2			
O_3	+ NO_2		$\rightarrow NO_3$	+ O_2			
N_2O_5	+ $h\nu$		$\rightarrow 2NO_2$	+ O			
N_2O_5	$\rightarrow NO_3$	+ NO_2					

Table II lists additional reactions which might possibly affect the accuracy of J_M values derived from Equation (7). The potential effect of species present in small concentrations during the photolysis is best illustrated by examining the overall quantum yield for the removal of NO_2. In the simplified mechanism each oxygen atom produced by primary photodissociation of NO_2 is assumed to remove another NO_2 molecule, so that the overall quantum yield equals 2. In practice, other oxygen atom removal processes also occur and so may other pathways for the reformation of NO_2.

The rate equation for NO_2 disappearance can be written in the form

$$\frac{d[NO_2]}{dt} = -\phi_1 J_M [NO_2] \tag{14}$$

where the quantum yield ϕ_1 includes the appropriate rate terms for all the reactions included in Table II; ϕ_1 was calculated by numerical integration using recommended rate constants for these reactions, and is shown in Figure 3 as a function of $2J_M t$. It is seen to differ from 2 by less than 2% for $2J_M t < 3$. Since highest statistical weight is given to measurements at early stages of photolysis in the data analysis described below, the effects of these reactions are believed to be negligible, and estimated to introduce an error in J_M no greater than +0.4%.

Separate attention was given to the reformation of NO_2 by the recombination reaction

$$2NO + O_2 \longrightarrow 2NO_2 . \tag{R6}$$

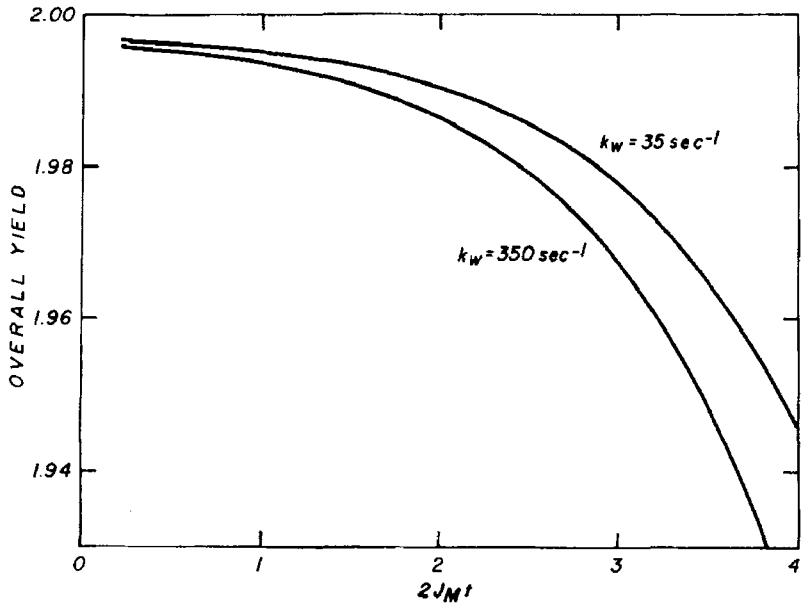

Fig. 3. The overall photodissociation yield (ϕ_1) of NO_2 calculated for two values of the oxygen atom wall loss rate.

The rate of NO_2 formation resulting from reactions (R1), (R2) and (R6) can be written as

$$\frac{d[NO_2]}{dt} = -2J_M[NO_2] + 2k_6[NO]^2[O_2] \equiv \phi_2 J_M[NO_2]. \tag{15}$$

The effective quantum yield, ϕ_2 is time dependent and equals 2 at the beginning of the photolysis and eventually goes to zero when the photolysis rate equals the rate of recombination. Values of ϕ_2 were calculated by numerical integration of Equation (15) for the case of $p_{NO_2}(0) = 2$ torr and $J_M = 10^{-2}\ s^{-1}$. The calculations show that ϕ_2 decreases by 15% at the end of a typical photolysis experiment lasting 180 s. However, by this time NO_2 has decreased to 3% of its initial value and therefore the data plotted according to Equation (7) shows a slight deviation from linearity only at the longer times.

Furthermore, as mentioned above, J_M is determined from a least squares fit that gives greater statistical weight to pressure measurements made at the early stages of the photolysis, where ϕ_2 is very close to 2. We therefore conclude that reaction (R6) does not significantly affect the measured pressure increase attributed to photolysis.

The recombination reaction (R6), also affects $\Delta P(\infty)$ required in Equation (8). As $t \longrightarrow \infty$, p_{NO_2} reaches an equilibrium value given, to a close approximation, by:

$$p_{NO_2}(eq) = p^3_{NO_2}(0)k_6/2J_M. \tag{16}$$

The correction to $\Delta P(\infty)$, estimated for our experimental conditions using Equation (16), was found to be always smaller than the 40 mtorr experimental uncertainty in

$\Delta P(\infty)$ and was typically less than 10 mtorr. Therefore the recombination was not included in the data reduction.

This conclusion was verified experimentally in a number of ways: (1) J_M values for a number of experiments were calculated with and without the correction for the recombination reaction using an iterative numerical analysis. Agreement with 2% was obtained in all cases. (2) The values of J_M obtained without correcting for the recombination were found to be independent of $p_{NO_2}(0)$ over the range 0.7 – 3.1 torr. (3) After completion of an experiment, when the cell was covered, the small observed rate of pressure decrease was consistent with the values calculated from Equation (15). The back reaction is estimated to decrease the photolysis rate in the cell by less than 2%.

Finally, consideration was given to possible reactions of excited NO_2 molecules (NO_2*) produced by absorption in the 400–500 nm range,

$$NO_2^* + NO_2 \longrightarrow \text{products} \qquad \text{(R7)}$$

$$NO_2^* \xrightarrow{\text{walls}} \text{products}$$

A calculation, including self quenching and several product channels, has shown (Madronich, 1982) that this reaction should contribute at most 1.5% to J_M. Furthermore, several photolysis experiments were performed (under Xe lamp illumination) with N_2, a strong quencher of NO_2*, added over the range 0 to 12 torr. J_M was found to be independent of N_2 pressure, showing that, for broadband illumination, excited NO_2 molecules play no significant role in the overall photodissociation rate. Reactions with excited species are estimated to increase the photolysis rate in the cell by less than 1.5%. These experiments also indicate that J_M is not pressure dependent, in agreement with the findings of Dickerson *et al.* (1982).

The overall uncertainty in J_M resulting from the neglect of reactions (R4) to (R7) in Equation (7) can be estimated by combination of the uncertainties discussed above. It amounts to (+2%, –1.6%). To be conservative, we raise the uncertainty due to simplified kinetics to (+2.5%, –2%) to include any deviation from the steady-state assumption used to derive Equation (7).

5. Optical Considerations

To transform the measured photodissociation coefficient, J_M, to the atmospheric solar photodissociation coefficient, J_{NO_2}, it is necessary to consider possible perturbations of the ambient light by the cell optics. Reflection and refraction occur at the quartz/air/quartz/NO_2 interfaces and the mechanical supports of the instrument shadow parts of the cell volume.

The effect of refraction is illustrated in Figure 4. An incoming ray is refracted at each interface and traverses a length L_1 (A-B) in the photolysis cell (the innermost circle of the diagram). In the absence of the quartz tubing the same ray would traverse a length L_0 (C-D). It is readily shown, by application of Snell's law at each interface and of the

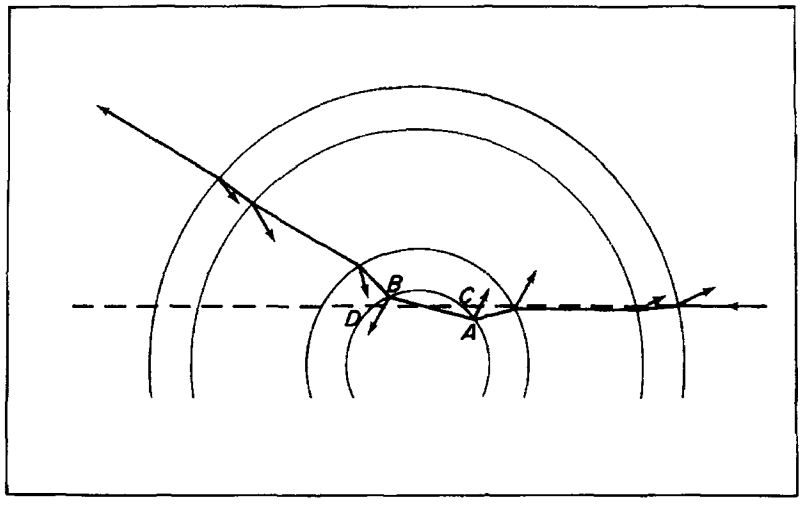

Fig. 4. Refraction geometry for the double walled photolysis cell shown in circular cross-section. The dashed line is the direction of the unrefracted incoming ray. The solid line represents the rays with refraction and some reflections. The differences in the indices of refraction have been exaggerated.

'law of sines' between successive interfaces, that L_0 and L_1 are equal for arbitrary incidence, provided the length of the cell is much greater than the thickness of the quartz and that the small difference between the indices of refraction of air and NO_2 are neglected. Thus, only the direction of the incoming ray is changed by refraction but the photodissociation rate is unaffected.

The effect of reflection in the double quartz cylinder was determined by ray-tracing, using an approach similar to that used by Zafonte *et al.* (1977) for a single wall, infinitely long, cylinder. For an infinitely long, non-absorbing, double-walled cell the reflection losses are also compensated by multiple internal reflections for all angles of incidence (Madronich, 1982). For a cell of finite length, some light loss is expected due to the truncation of internal reflections at the cell ends. For rays nearly parallel to the quartz tube axis, these losses may be significant, but the direction of incidence of these rays represents only a small fraction of the 4π steradian field of view. In practice, these rays are blocked before entering the quartz tubes by the fittings which are placed at or near the cell ends. The correction for this shadowing effect is discussed below.

As a test for the compensating effects of multiple reflections a series of experiments were performed in which J_M was measured with and without the outer quartz tube under conditions of essentially constant insolation as measured by an Eppley radiometer. Table III shows that within the uncertainty of the measurements there is no difference between a single and a double walled cell as expected on the basis of the reflection/refraction analysis discussed above. Similar findings were reported by Dickerson *et al.* (1982).

To obtain values of J_{NO_2}, the measured J_M values must be corrected for the fraction of the volume that is not fully illuminated. This includes the 'dead' volume of the tube connections to the cell (4% of the cell volume) and the volumes near the ends of the cell which are completely shadowed from direct sunlight but only partially from scattered

Table III. The effect of multiple reflections on J_M. 18 June 1981: solar zenith angle ≈ 30°; background: cement

Local time	$J_M \times 10^3$ s	Eppley (mW/cm²)
12 : 49	6.39 ± 0.27[a]	4.02
13 : 00	6.30 ± 0.31	3.99
13 : 10	6.37 ± 0.31[a]	4.02
13 : 24	6.32 ± 0.33	4.02
13 : 39	6.44 ± 0.32[a]	4.02

[a] Experiments using double walled cell; others have the outer quartz tube removed.

light. Shadowing, of course, decreases the average number of molecules dissociated per second. Since the rate of diffusion at the cell pressures of our experiments far exceeds the rate of photodissociation this decrease is related to the ratio of the shadowed to the total volume. However, the correction for shadowing depends not only on the geometry of the instrument but also on the direction of the incoming light. In general J_{NO_2} may be written in terms of three components, viz.

$$J_{NO_2} = J_o + J_u + J_d \tag{17}$$

where J_o, J_u, and J_d are the photodissociation coefficients for direct, upward scattered and downward scattered light, respectively. Thus,

$$J_M = f_o J_o + f_u J_u + f_d J_d \tag{18}$$

where f_i represents the fraction of the total cell volume illuminated by light component, i. If weight factors $w_i = J_i/J_{NO_2}$ are also defined then:

$$J_{NO_2} = \frac{J_M}{f_o w_o + f_u w_u + f_d w_d}. \tag{19}$$

The weight factors were estimated from an isotropic multiple scattering model described by Madronich *et al.* (1983) and are shown in Figure 5 for a range of surface albedos. Use of anisotropic scattering models (e.g., Isaksen *et al.*, 1977) resulted in slightly different factors which, however, resulted in differences in J_{NO_2} which were less than the experimental uncertainties.

Values of f_i are specific to the geometry and orientation of the instrument. Since the direct solar beam casts a sharp shadow, f_o was determined from the geometry of the fittings and the insulation surrounding the ends of the cell. For a vertical cell:

$$\begin{aligned} f_o &= (0.88 \pm 0.01) - (0.037 \pm 0.006) \cot\theta, \quad \text{for } 30° < \theta < 90°; \\ f_o &= (0.95 \pm 0.01) - (0.079 \pm 0.010) \cot\theta, \quad \text{for } 5° < \theta < 30° \end{aligned} \tag{20}$$

where θ is the angle between the cell axis and the incoming solar rays. The calculation of f_u and f_d is more complex because a knowledge of the hemispherical distribution of the

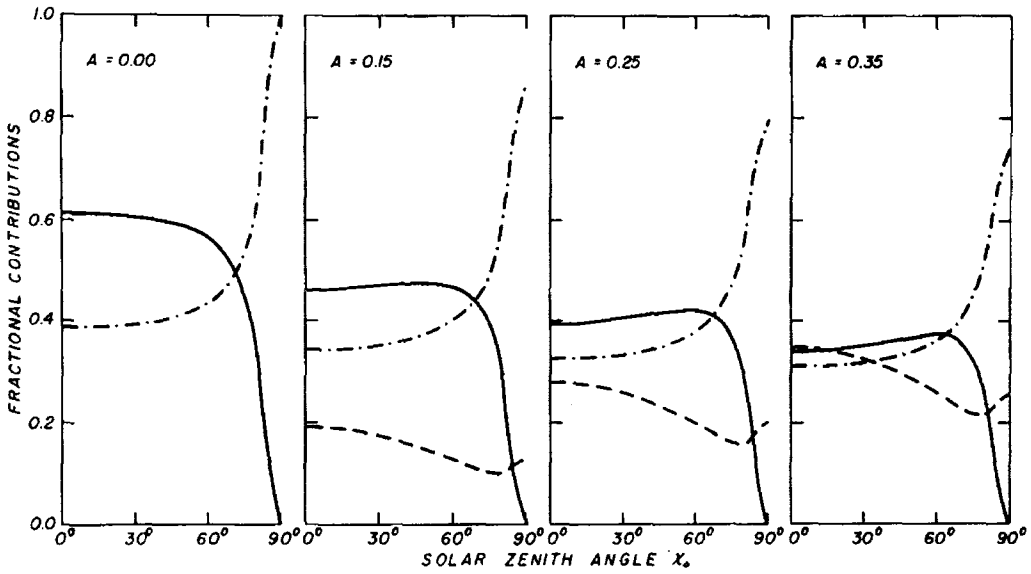

Fig. 5. Fractional contributions to J_{NO_2} calculated for the isotropic model. (—) direct Sun, w_o (-•-) downwelling radiation, w_d (---) upwelling radiation, w_u.

incoming fluxes is required. If both the upward and downward scattered light are assumed to vary only with azimuth, the average fraction of the cell volume that is illuminated by each component can be determined by integrating the unshadowed field of view along the axis of the cell. For the cell in the vertical position the calculations give:

$$f_u = 0.68 \pm 0.03 \tag{21}$$

$$f_d = 0.87 \pm 0.02. \tag{22}$$

The fractions f_u and f_d differ from each other because the instrument is suspended vertically about 5 m below a large balloon gondola and therefore its electronics and gas reservoirs shadow the bottom of the cell from upwelling radiation. The instrument is reeled up into the gondola before terminating the flight. This restricted the length of the instrument, making all the shadowing fractions appreciably less than unity. For surface measurements the choice of a longer quartz cell would obviously reduce the shadowing corrections.

For surface measurements, the cell was suspended over grass or black cloth. In both cases the 'local' albedo is close to zero and so, therefore, is the upwelling radiation striking the cell directly. The 'regional' (up to several 100 km^2) albedo will not be zero. Upwelling radiation from this region will, by scattering, contribute only to the downwelling radiation striking the cell. Under these conditions, Equation (17) becomes:

$$J_{NO_2} = J_M \frac{(w_o + w_d)}{f_o w_o + f_d w_d}. \tag{23}$$

In some of our experiments the photolysis tube was suspended horizontally. Because of cylindrical symmetry, f_u and f_d are identical in this orientation and have a value equal

to the average of the two given above for the vertical suspension. Expression (20) for f_o remains unchanged and

$$J_{NO_2} = J_M \frac{(w_o + w_d)}{f_o w_o + \frac{1}{2}(f_u + f_d) w_d} . \tag{24}$$

Values of w_o and w_d were obtained from the model using a regional albedo of 0.25.

For the range of solar zenith angles and cell orientations used in the ground measurements the shadowing corrections varied from 20 to 30%, i.e., $J_{NO_2} = (1.2 \text{ to } 1.3) J_M$, the largest correction applying to measurements near sunset. For instruments designed specifically for ground based measurements practical choices of the ratio of length to diameter of the cell could reduce the correction to less than 2%.

The uncertainty in the shadowing correction has two components. One is in the calculation of the w_i values, which requires a choice of regional albedo. The model was tested for sensitivity to this choice which led to the conclusion that the maximum uncertainty it introduced to J_{NO_2} was 0.5%. The validity of the model itself in evaluating w_i could not be tested directly but its ability to reconcile J_{NO_2} values with photometric UV measurements, as described below, indicated that it does not introduce significant uncertainties in the shadowing corrections.

The other uncertainty involves the illumination fractions, f_i. This was estimated from the uncertainties in the physical dimensions of the instrument and the propogation of these uncertainties through the appropriate geometric functions used to calculate f_i. The

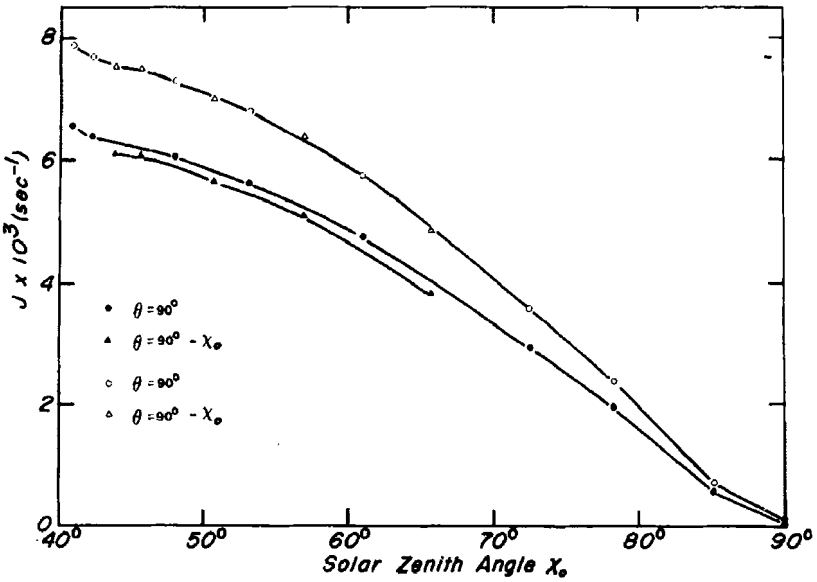

Fig. 6. The effects of shadowing correction using different cell orientations. Solid symbols are values of J_M. Open symbols are values of J_{NO_2}. The angle between the cell axis and the sun (θ) is given in terms of the solar zenith angle.

uncertainties in the f_i's contributed at most a 2.5% uncertainty to the correction factor J_{NO_2}/J_M. The overall uncertainty in J_{NO_2} arising from the shadowing correction is estimated to be ±2.5%.

A series of experiments were performed to test for optical perturbations of the double-walled cell. The orientation of the axis of the cell relative to the solar meridional plane was varied from 0° to 90°. Figure 6 shows that J_{NO_2} is insensitive to the direction of the incoming light when the shadowing correction is applied. This confirms both the validity of the correction and the analysis which showed the reflection and refraction perturbations to be negligible.

Finally, the ambient light may be attenuated by the NO_2 present in the cell. An accurate correction for this light loss is impractical, due to the wavelength variation of the NO_2 absorption cross-section and to the difficulty of computing optical pathlengths for direct and diffuse fluxes and their internal reflections. Based on a value of 5×10^{-19} cm^2 for the average NO_2 cross-section and on values of w_o and w_d of Figure 5, we estimated that the attenuation is less than 4% for all measurements reported here, and is usually in the range 1.5–2.0%. These estimates were not applied as correction factors to J_{NO_2}, but were included as part of the total uncertainty of J_{NO_2} measurements.

6. Ground-Based Measurements of J_{NO_2}

Four sets of ground level measurements of J_{NO_2} were made at Toronto, Canada (43.5°N, 79.5°W, 200 m ASL).

On 26 June, 1980, the cell was mounted vertically, 1 m above a grass surface. The albedo of grass has been determined by Harvey *et al.* (1977) to be less than 0.01 in the near UV; local reflections are therefore negligible.

On 27 March, 20 August and 21 August 1981, the instrument was located on the roof of a building, with the cell mounted horizontally, about 15 cm above a black cloth. Seen from this location, surrounding buildings rise less than 15° above the horizon and obstruct less than 10% of the sky. On the two days in August the cell axis was held perpendicular to the direction of the solar beam; on 27 March, the sun-tube angles varied from 24° to 90°.

In each of the experiments, the cell was filled with NO_2, while it was covered by the shutter or, in the case where it was mounted horizontally, by black cloth. The cell was then exposed to daylight and the pressure increase monitored. The exposure was continued for 5 to 10 min to ensure establishment of the final pressure, $P(\infty)$. The cell was then evacuated into the 7 ℓ reservoir and refilled for the next measurement. Measurements were taken at approximately 20 min intervals. The temperature of the cell was constant within 0.5° during each experiment.

The pressure increase for the first 180 s of each photolysis was plotted according to Equation (7) and shown in Figure 2. The slope of this plot, $2J_M$, was derived by a least-squares method and takes into account the statistical importance of measurements having different uncertainties. Since the photolysis is first order in p_{NO_2}, measurements made at longer times are less important that those made near the beginning of the photo-

lysis. Each measurement was therefore weighted, in the least squares fit, by the square of the reciprocal of its uncertainty.

Precision estimates for $P(0)$, $\Delta P(t)$ and $\Delta P(\infty)$ were ±0.01, ±0.005 and ±0.005 torr, respectively. These uncertainties, assumed to be independent, were propagated, one at a time, through the kinetic expressions (7) to (11) to obtain the error bars for each measurement, as shown in Figure 2. The precision of J_M, was calculated from the least-squares variance and ranged from ±1% at the highest pressures to ±4% at the lowest pressures.

In addition to random errors there were a number of sources of systematic errors associated with the measurements which have been identified. Contributions to the error in $P(0)$ include upper limits of ±0.030 torr from the zero offset of the pressure transducer and −0.010 torr from surface adsorption of NO_2. The total systematic error in $P(0)$ is estimated to be less than ±0.04 torr. The uncertainty in $\Delta P(\infty)$ includes ±0.005 torr from the calibration of the pressure transducer and +0.010 to +0.030 torr from surface adsorption for a total of ±0.04 torr.

Each J_M value, computed by the weighted least-squares method, was tested for sensitivity to the systematic errors in $P(0)$ and $\Delta P(\infty)$. The combined effect of these systematic instrumental errors ranged from 3 to 10%, with the highest errors occurring for the lowest initial pressures.

The total uncertainty for each value of J_M was calculated by combining the uncertainties due to: (1) those calculated from the least square variance; (2) the systematic errors; (3) the neglect of kinetic mechanisms other than those leading to Equation (7); (4) the shadowing correction; (5) the flux attenuation due to the NO_2 in the cell. These uncertainties were assumed to be independent and normally distributed. The total uncertainty in J_{NO_2} ranged from ±6.5% to ±13.3%.

7. Results

The measured J_{NO_2} values are shown as a function of zenith angle in Figure 7. For clarity, error bars are shown only for the data of 27 March, 1981; the relative errors for the other measurements are comparable.

The highest values of J_{NO_2} were observed on the day of clearest sky conditions (27 March). Values of 5% to 10% lower were obtained on days with hazier skies (20 and 21 August), for zenith angles less than about 60°; haze was less important for larger zenith angles. Five of the measurements on 26 June 1980, were made when the Sun was blocked by clouds and four when only some blue sky light was obscured by cloud. All the measurements fall below clear sky values obtained on other days which illustrates the difficulty of predicting J_{NO_2} for partly cloudly conditions.

Detailed comparisons between our measurements and those of other workers are not too meaningful in view of the differences in surface albedos and meteorological conditions. However, there is reasonable agreement among the higher J_{NO_2} values reported for clear sky conditions. Thus, our value of $8.0 \times 10^{-3}\ s^{-1}$ for a solar zenith angle χ_0 of 40° compares favourably with the values of $8.3 \times 10^{-3}\ s^{-1}$ for $\chi_0 \simeq 30°$ by Zafonte *et al.* (1977), $8.7 \times 10^{-3}\ s^{-1}$ for $\chi_0 = 30°$ and $8.3 \times 10^{-3}\ s^{-1}$ at $\chi_0 = 40°$ by Harvey *et al.* (1977) and

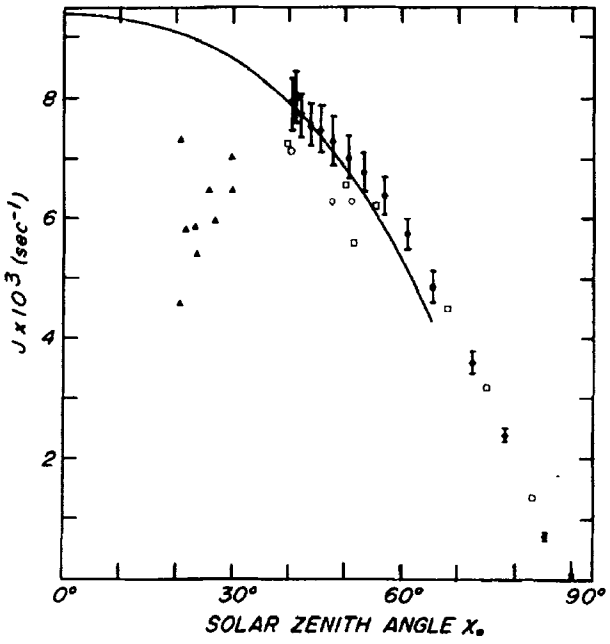

Fig. 7. Experimental values of J_{NO_2} (▲) 26 June, 1980; (●) 27 March, 1981; (□) 20 August, 1981, (○) 21 August, 1981. The solid curve represents measurements reported by Dickerson *et al.* (1982).

a mean value of 8.0×10^{-3} s^{-1} with a maximum of 8.8×10^{-3} s^{-1} at $\chi_0 \simeq 29°$ by Bahe *et al.* (1980). Values as high at 1.0×10^{-2} s^{-1} were observed by Dickerson *et al.* (1982) but these were obtained at smaller zenith angles and higher altitudes. For χ_0 in the range of 30°–40° they report values from 8 to 9×10^{-3} s^{-1}. Their empirical fit between J_{NO_2} and χ_0 is shown on Figure 7. This curve represents our data reasonably well for χ_0 between 40° and 50° but lies below our measurements for larger zenith angles.

Comparisons with the measurements of Dickerson *et al.* (1982) may not be too meaningful, however. These authors measured the temperature dependence of J_{NO_2} and found it to be very small and in reasonable agreement with calculations based on the temperature dependence of the absorption coefficients and quantum yields measured by Davenport *et al.* (1978) over the wavelength interval from 390 to 420 nm. However, detailed calculations by Madronich *et al.* (1983) showed that only one-third of the temperature dependence occurs in this wavelength region while two-thirds occurs at shorter wavelengths. The small temperature dependence observed by Dickerson *et al.* (1982) is therefore difficult to understand.

7.1. *Comparison of J_{NO_2} with Eppley measurements*

Simultaneously with the J_{NO_2} measurements downwelling radiation was monitored with a calibrated, Eppley UV (295–385 nm) radiometer pointed towards the zenith. The correlation between the Eppley readings and the measured J_{NO_2} values is shown in Figure 8. Similar correlations were reported by other groups and our results are in good agreement

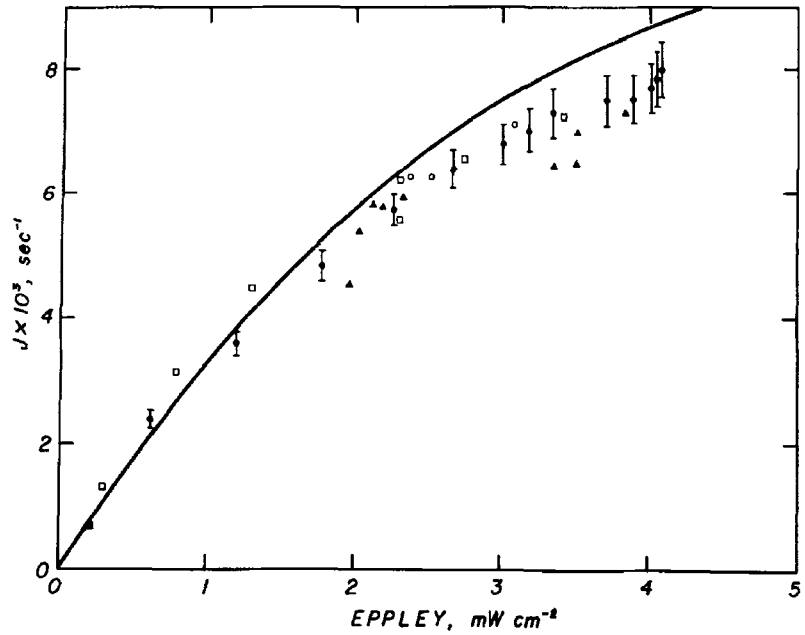

Fig. 8. Correlation between experimental J_{NO_2} values and Eppley radiometer readings. The symbols correspond to those used in Figure 7. The solid curve is taken from Harvey *et al.* (1977).

with those of Zafonte *et al.* (1977). The correlation curve given by Harvey *et al.* (1977) is shown in Figure 8 for comparison. For large Eppley signals, their J_{NO_2} values are consistently some 10% higher than ours, while for lower Eppley signals, good agreement is obtained only for clear sky data. This may be due, in part, to the higher (*ca.* 10%) local albedo present during their measurements. Lambertian reflections from a high albedo surface are greatest for small zenith angles, corresponding to large values of J_{NO_2} and Eppley readings. Correlations between J_{NO_2} and radiometer readings were also reported by Bahe *et al.* (1980) but cannot be compared with our data because the spectral response of their radiometer differs from that of the Eppley. They report a similar curved correlation for data obtained on any clear day but a broad linear correlation for the average of measurements made over many days having a variety of atmospheric conditions.

Non-linearity in the correlation between the Eppley readings and J_{NO_2} is due, mainly, to the difference between the responses of the two instruments to the direction of the incoming light. The Eppley signal is proportional to the energy crossing the flat detector surface and is, therefore, a function of the angle between the detector and the incoming light, θ:

$$E = \int A(\lambda) \iint I(\lambda, \theta, \phi) \cos\theta \sin\theta \, d\theta \, d\phi \, d\lambda \tag{25}$$

where E is the Eppley signal, $A(\lambda)$ is the Eppley spectral response function, $I(\lambda, \theta, \phi)$ the spectral radiance ($mW/cm^2 \cdot nm \cdot sr$) and ϕ the azimuthal angle. J_{NO_2}, on the other hand, is independent of the direction of the incoming light and is given by:

$$J_{NO_2} = \int B(\lambda) \iint I(\lambda, \theta, \phi) \sin\theta \, d\theta \, d\phi \, d\lambda \tag{26}$$

where $B(\lambda)$ is given by the NO_2 absorption coefficient and the primary quantum yield.

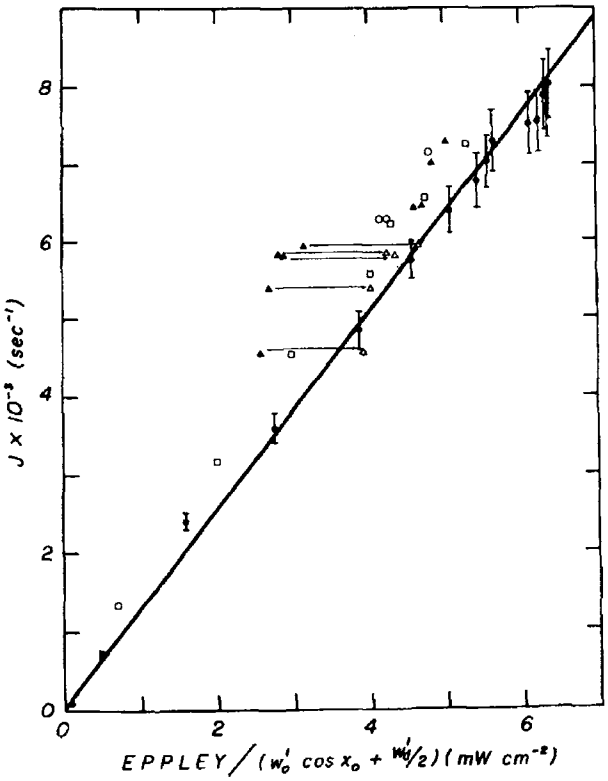

Fig. 9. Correlation between J_{NO_2} and adjusted Eppley readings. (△) are corrected (▲) for the absence of direct sunlight. All other symbols are as in Figure 7.

Evaluation of the angular integrals in Equations (25) and (26) requires the knowledge of the angular distribution of the light from the overhead hemisphere. If the diffuse light is assumed to be isotropic the equations yield:

$$\frac{E}{J_{NO_2}} = w_o \cos\chi_0 \frac{\int A(\lambda) I_o(\lambda)\, d\lambda}{\int B(\lambda) I_o(\lambda)\, d\lambda} + \frac{1}{2} w_d \frac{\int A(\lambda) I_d(\lambda)\, d\lambda}{\int B(\lambda) I_d(\lambda)\, d\lambda} \tag{27}$$

where $I_o(\lambda)$ and $I_d(\lambda)$ are the spectral radiances of direct and diffuse light, respectively and χ_0 is the solar zenith angle.

If the functions $A(\lambda)$ and $B(\lambda)$ are nearly constant over the spectral region of interest, the correlations between the Eppley signals and J_{NO_2} can be approximated by:

$$\frac{E}{J_{NO_2}} = C(w_o \cos\chi_0 + \frac{1}{2} w_d) \tag{28}$$

where C is independent of the intensity or direction of the incoming light. This new correlation is plotted on Figure 9 and shows much better linearity than Figure 8. The only significant deviation from linearity occurs when the Sun is blocked by cloud. This is not surprising, since the direct sun component, w_o, was calculated for clear sky conditions; little direct sunlight is observed by either instrument when the Sun is obscured by cloud. If the remaining light, from broken clouds and patches of blue sky, is assumed to be isotropic, values of $w_o = 0$ and $w_d = 1$ should be used in Equation (28). Values for

obscured Sun conditions, recalculated this way, and shown in Figure 9, agree well with the correlations obtained with full Sun illumination.

J_{NO_2} values obtained when the Sun was not obscured, but with the sky either hazy or partly cloudy, fall somewhat above the line defined by the clear sky data of 27 March, 1981. Two reasons may be proposed to explain this behaviour. First, the ambient temperature on 27 March, 1981 was some 15 to 25°C lower than on the days of the other measurements. These lower temperatures would result in a reduction of J_{NO_2} because of the temperature dependence of the NO_2 absorption cross-section and photodissociation yield. Second, the relative importance of scattered and direct solar radiation is different for clear, hazy and partly-cloudy conditions.

7.2. *Comparisons of Measurements with Theory*

The experimental values of J_{NO_2} are compared, in Figure 10, with values calculated by two simplified radiative transfer models. One model is based on the columnar scattering approximation of Isaksen *et al.* (1977) and the other is based on the suggestion of Luther (1980) of isotropic propogation for scattered and reflected light. Only the downwelling contributions are included in the calculations since the experiments were performed over black cloth or grass, both of which have negligible albedo.

The figure shows agreement better than 15% between the isotropic model calculations and the measured values at all zenith angles, except for partly cloudy conditions. The predictions of the columnar model of Isaaksen *et al.* (1977) also agree well with the

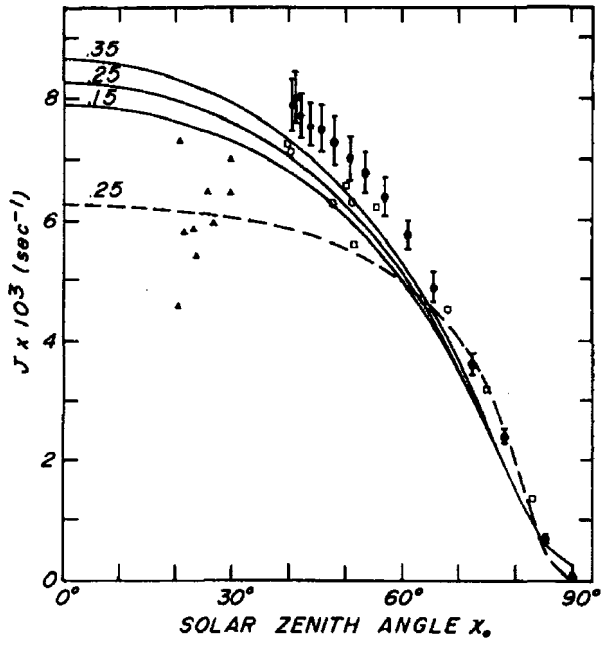

Fig. 10. Comparison between experimental and theoretical J_{NO_2} values. Symbols are the same as in Figure 7. Solid and dashed lines are isotropic and columnar model results, respectively. The global albedo used in each calculation is indicated, but only the downwelling contributions to the calculated J_{NO_2} values are shown.

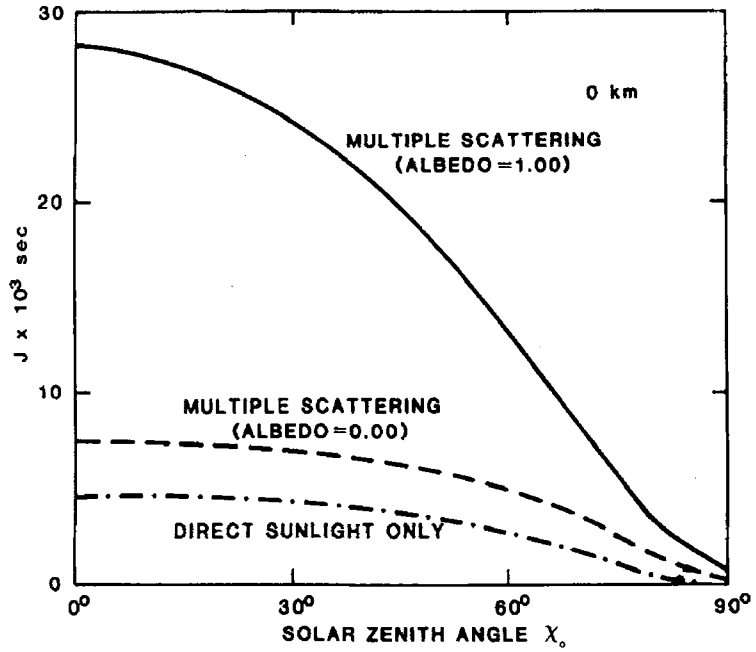

Fig. 11. Sensitivity of calculated J_{NO_2} values to isotropic model parameters.

measurements for $\chi_0 > 65^\circ$, but are some 30% smaller than the measured values at smaller zenith angles.

Measurements obtained under the very clear sky conditions of 27 March are consistently some 10% larger than the isotropic model values, which could be due to some local albedo, from the adjacent grey-top roof and from nearby buildings.

8. Discussion

NO_2 is more sensitive than most atmospheric species to the effects of scattering and reflections, since it is photodissociated mainly in the wavelength region between 300 and 420 nm. Although this spectral region is relatively free of atmospheric absorption, reflections and Rayleigh scattering redistribute much of the incoming sunlight. If only direct sunlight were effective, Figure 11 shows that the maximum value of J_{NO_2} is less than 5×10^{-3} s^{-1} for the isotropic model. If diffuse light, arising from multiple scattering is included, J_{NO_2} can increase to about 7×10^{-3} s^{-1}. If, in addition, all of the light which reaches the ground is reflected isotropically, J_{NO_2} values as high as 2.8×10^{-2} s^{-1} are calculated due, largely, to the 2 cos χ_0 factor associated with Lambertian reflection. Other calculations of J_{NO_2} (e.g., Luther and Gelinas, 1976) show similar albedo and scattering effects. Recent calculations of the actinic flux by Nicolet *et al.* (1982) show that the extraterrestrial flux at 360 nm is enhanced by a factor of 4.25 at 0 km, $\chi_0 = 0$ deg and albedo = 1.0. In view of the sensitivity of the theory to atmosperic and surface conditions the agreement between measurement and theory shown in Figure 10 and the ability of the theory to 'bring into line' Eppley and J_{NO_2} measurements is gratifying. The

agreement is not, however, good enough for theoretical values of J_{NO_2} to be used in models of the troposphere or to test the validity of the photochemical steady-state expression (1). Measured values of J_{NO_2} are to be preferred especially in cases of high or variable scattering.

Measured J_{NO_2} values, of course, are only applicable to conditions under which they have been obtained. For example a measurement made on the rooftop of a building will be influenced by the local albedo of the roof. But the local albedo affecting a measurement made 100 m above the roof will include contributions from adjacent buildings, trees, etc. Differences in local albedo and haze conditions make it difficult to compare the J_{NO_2} measurements reported by different workers.

Estimates of J_{NO_2} may be obtained with an accuracy of about 20% from Eppley radiometer readings if a calibration curve such as that shown in Figure 9 is available. Care must be taken, however, in using such a correlation, since the Eppley and J_{NO_2} instruments differ both in their spectral responses and in their sensitivity to the direction of the incoming light.

Acknowledgments

The authors wish to thank the Atmospheric Environment Service of Canada and the National Sciences and Engineering Research Council of Canada for financial assistance.

References

Bahe, F. C., Schurath, U., and Becker, K. H., 1980, The frequency of NO_2 photolysis at ground level, as recorded by a continuous actinometer, *Atmos. Environ.* 14, 711–718.

Davenport, J. E., 1978, Determination of NO_2 photolysis parameters for stratospheric modelling, FAA Report No. FAA-EQ-7-14.

Dickerson, R. R., and Stedman, D. H., 1980, Precision of NO_2 photolysis rate measurements, *Environ. Sci. Tech.* 14, 1261–1262.

Dickerson, R. R., Stedman, D. H., and Delany, A. C., 1982, Direct measurements of ozone and nitrogen dioxide photolysis rates in the troposphere, *J. Geophys. Res.* 87, 4933–4946.

Harvey, R. B., Stedman, D. H., and Chameides, W., 1977, Determination of the absolute rate of solar photolysis of NO_2, *J. Air Pollution Control Assoc.* 27, 663–666.

Holmes, H. H. and Daniels, F., 1934, The photolysis of nitrogen oxides: N_2O_5, N_2O_4, and NO_2, *J. Am. Chem. Soc.* 56, 630–637.

Isaksen, I. S. A., Midtbo, K. H., Sunde, J., and Crutzen, P. J., 1977, A simplified method to include molecular scattering and reflection in calculations of photon fluxes and photodissociation rates, *Geophys. Norveg.* 31, 11–26.

JPL, 1982: *Chemical Kinetic and Photochemical Data for Use in Stratosphere Modelling: Evaluation Number 5*, JPL Publication 82–57, Pasadena, California.

Jackson, J. O., Stedman, D. H., Smith, R. G., Hecker, L. H., and Warner, P. O., 1975, Direct NO_2 photolysis rate monitor, *Rev. Sci. Instr.* 46, 376–378.

Johnston, H. S., and Graham, R., 1974, Photochemistry of NO_x and HNO_x compounds, *Can. J. Chem.* 52, 1415–1423.

Luther, F. M., 1980, Annual Report of the Lawerence Livermore National Laboratory to the FAA, UCRL-50042-80, Lawerence Livermore Laboratory, Livermore, California.

Luther, F. M. and Gelinas, R. J., 1976, Effect of molecular multiple scattering and surface albedo on atmospheric photodissociation rates, *J. Geophys. Res.* 81, 1125–1132.

Madronich, S., 1982, Measurements of the photodissociation coefficient of NO_2 in the stratosphere, PhD Thesis, York University.

Madronich, S., Ridley, B. A., Hastie, D. R., and Schiff, H. I., 1983, Calculation of the temperature dependence of the NO_2 photodissociation coefficient in the atmosphere, *J. Atmos. Chem.* 1, forthcoming.

Mugnai, A., Petroncelli, P., and Fiocco, G., 1979, Sensitivity of the photodissociation of NO_2, NO_3, HNO_3 and H_2O_2 to the solar radiation diffused by the ground and by atmospheric particles, *J. Atmos. Terr. Phys.* **41**, 351–359.

Nicolet, M., Meier, R. R., and Anderson, D. E., Jr., 1982, Radiation field in the troposphere and stratosphere-II. Numerical analysis, *Planet. Space Sci.* **30**, 935–983.

WMO, 1981: The stratosphere 1981: Theory and measurements, WMO Global Ozone Research and Monitoring Project. Report No. 11, May 1981.

Zafonte, L., Rieger, P. L., and Holmes, J. R., 1977, Nitrogen dioxide photolysis in the Los Angeles atmosphere, *Environ. Sci. Tech.* **11**, 483–487.